Supplementary Information

Hybrid graphenic and iron oxide photocatalysts for the decomposition of synthetic chemicals

Raphaell Moreira[1,2*], Ehsan B. Esfahani[1], Fatemeh A. Zeidabadi[1], Pani Rostami[1], Martin Thuo[3], Madjid Mohseni[1], Earl J. Foster[1*]

Table S1. Literature data on PFOA degradation using UV (254 nm) photo-chemical/catalytic processes.

Experimental conditions	PFOA concentration (mg/L)	Process	Decomposition (%)	Irradiation time (h)	Ref.
18 W LP-Hg lamp (254 nm) Catalysts dose: 1.0 g/L pH no adjustment Fluence rate = 1.42 mW/cm^2 = 0.56 W/L	0.1 0.5 1 5 50	UV/Fe_2O_3/g-NC	92.1 82.8 75.9 69.7 60.0	1.5	This Study
Heterogenous catalysts					
5 W UV (254 nm) lamp Catalysts dose: 0.1 g/L pH 4.0 UV intensity (No information)	50	UV/$BiFeO_3$ UV/Pb-$BiFeO_3$ UV/Pb-$BiFeO_3$/rGO	~0% ~0% ~48%	8	[1]
18 W LP-Hg lamp (254 nm) Catalysts dose: 1.8 g/L pH ~4 UV intensity = 2.17×10^{-5} Es/(L.s) = 10.23 W/L	~54	UV/β-Ga_2O_3 UV/n-$BiPO_4$ UV/BiOHP	~25% ~30% ~100%	1	[2]
18 W LP-Hg lamp (254 nm) Catalysts dose: 1.0 g/L pH 7.0±0.1 Fluence rate = 21 mW/cm^2	0.2	UV/BiOHP UV/9%BiOHP/CS	66.2% ~100%	4	[3]
UV (254 nm) lamp (average fluence rate of 21 mW cm^{-2}) Catalysts dose: 1.0 g/L pH 7.0±0.3, 25 ℃	0.1	UV/TNTs@AC UV/calcined TNTs@AC UV/non-calcined TNTs@AC UV/Fe/TNTs@AC	23.8% 83.3% 68.7% 91.3%	4	[4]
400 W UV lamp (254 nm) Catalysts dose: 0.5 g/L Light intensity = 120,000 lux	50	UV/TiO_2 UV/Fe-TiO_2 UV/Cu-TiO_2	14% 69% 91%	12	[5]
23 W UV lamp (254 nm) Catalysts dose: 0.5 g/L UV intensity (No information)	41.4	UV/TiO_2 UV/In_2O_3	15.9% 80%	4	[6]
5 W UV lamp (254 nm) Catalysts dose: 0.5 g/L UV intensity (No information)	50	UV/SiC/graphene	45%	6	[7]
36 W LP-Hg lamp (254 nm) 3-indole-acetic-acid (IAA): 0.2 g/L Clay: 2.2 g/L	10	UV/IAA UV/IAA/Na-Montmorillonite	~35% ~20% 100%	5	[8]

UV intensity = 4.5 mW/cm^2		UV/IAA/HDTMA-Montmorillonite			
Molecular photo-mediators					
16 lamps (254 nm) with emission intensity of 8.0 mW. cm^{-2} for each lamp Sodium sulfite: 2.52 g/L pH 10	66	UV/sulfite	~90%	1	[9]
10 W LP-Hg lamp (254 nm) Sodium sulfite: 1.26 g/L pH 10.3 Fluence rate = 0.89×10^{-6} Es/(s) = 0.42 W	8.3	UV/sulfite	100%	2	[10]
14 W LP-Hg lamp (254 nm) Potassium iodide: 0.05 g/L pH 10 UV intensity (No information)	12.4	UV/iodide	99.8%	10	[11]
400 W LP-Hg lamp (254 nm) Sodium bicarbonate: 3.4 g/L Light intensity = 120,000 lux	50	UV/bicarbonate	100%	12	[12]
23 W LP-Hg lamp (254 nm) Ferric sulfate: 0.02 g/L UV intensity (No information)	19.8	UV/ferric	78.9%	4	[13]
16 W LP-Hg lamp (254 nm) Sodium persulfate: 3.6 g/L UV intensity = 2.88×10^{-7} Es/(L.s) = 0.14 W/L	62.1	UV/persulfate	85.6%	8	[14]
23 W LP-Hg lamp (254 nm) Sodium periodate: 3.6 g/L UV intensity = 62 mW/cm^2	4.14	UV/periodate	70%	2	[15]

1. Characterization of Fe/g-C hybrid photocatalyst

1.1 Scanning Electron Microscopy (SEM) and Thermogravimetric Analysis (TGA)

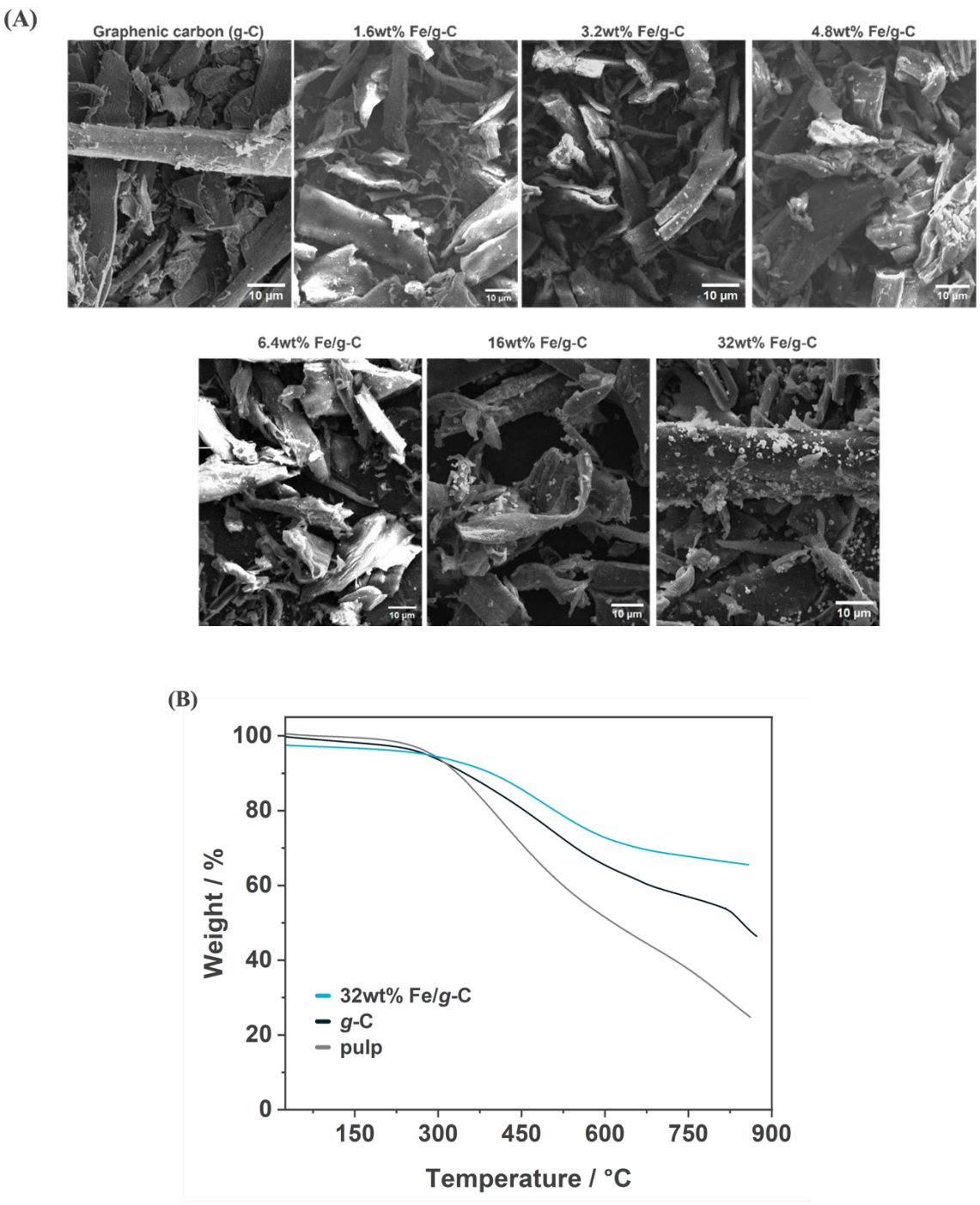

Figure S1: (A) SEM series of images showcasing the evolution of the photocatalyst hybrid as iron content is incrementally raised. (B) Thermogravimetric analysis of *g*-C and 32wt% Fe/*g*-C compared to strating material (e.g., pulp).

1.2 Fourier Transformed Infrared (FT IR) and Raman Spectroscopies

Table S2. Ratios of the *D* and *G* band intensities of the pure and iron oxide-loaded samples as function of iron content

Sample	I_D/I_G ratio
g-C	1.12
1.6wt% Fe	1.27
3.2wt% Fe	1.35
4.8wt% Fe	1.49
6.4wt% Fe	1.68
16wt% Fe	1.72
32wt% Fe	1.86

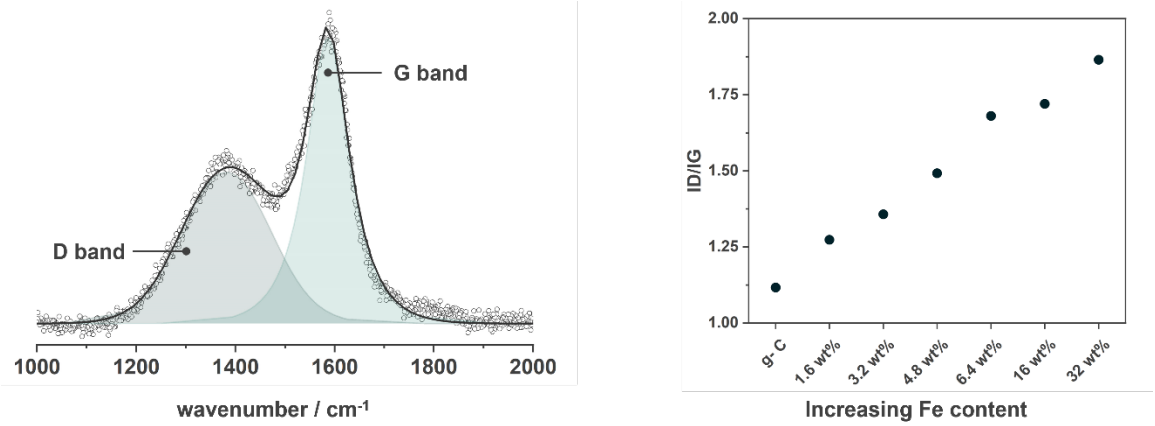

Figure S2. Fitting of Raman spectrum (left) for sample 16wt% Fe/*g*-C to obtain the I_D/I_G ratios (right).

1.3 Specific surface area and porosity

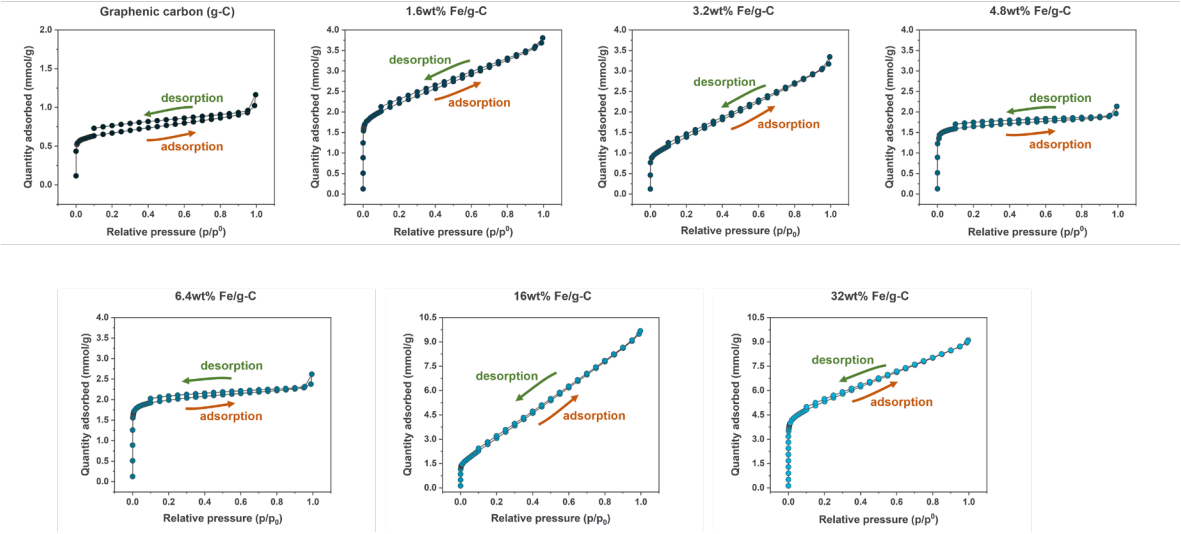

Figure S3. Detailed N_2 physisorption isotherm of the photocatalyst hybrids.

Table S3. Textural analysis values (specific surface area and pores volumes) of the Fe/*g*-C photocatalyst hybrids.

	g-C	**1.6wt% Fe/g-C**	**3.2wt% Fe/g-C**	**4.8wt% Fe/g-C**	**6.4wt% Fe/g-C**	**16wt% Fe/g-C**	**32wt% Fe/g-C**
S_{BET} / m^2g^{-1}	56	169	108	146	154	258	427
$S_{micro,\ t\text{-}plot}$ / m^2g^{-1}	40	89	87	128	137	198	223
$S_{external,\ t\text{-}plot}$ / m^2g^{-1}	16	80	99	13	16	76	199

$V_{p,\ total}$ / cm^3g^{-1}	0.033	0.122	0.104	0.007	0.078	0.314	0.293
$V_{p,\ micro}$ / cm^3g^{-1}	0.016	0.044	0.046	0.050	0.063	0.085	0.105

1.4 Diffusive Reflectance Spectroscopy (DRS)

Table S4. Values of optical bandgap calculated using Tauc of Fe/g-C photocatalyst hybrids.

Sample	Optical bandgap (E_g) / eV
g-C	1.28
1.6wt% Fe/*g*-C	1.43
3.2wt% Fe/*g*-C	1.49
4.8wt% Fe/*g*-C	1.39
6.4wt% Fe/*g*-C	1.33
16wt% Fe/*g*-C	1.26
32wt% Fe/*g*-C	1.19

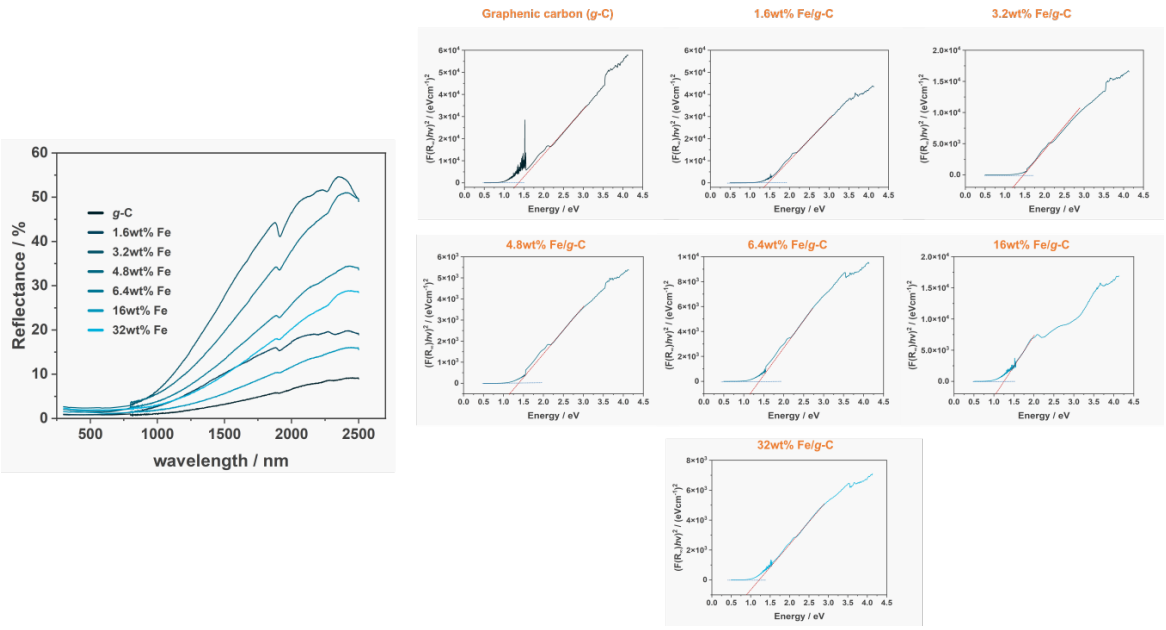

Figure S4. Diffusive reflectance spectra of the Fe/g-C photocatalyst hybrids (left) and Tauc representation for optical bandgap determination (right)

1.5 Photoelectron Spectroscopy (XPS)

Figure S5 and **Table S5** show the XPS data and fitting parameters for the *g*-C photocatalyst. The XPS spectra of C 1s and O 1s show all the oxygen-containing functional groups present on the carbon support. The main peaks in the C 1s spectrum correspond to carbon-carbon (C-C) bonds at approximately 284.6 eV, carbon-oxygen (C-O) bonds at around 286.3 eV, and carbonyl groups (C=O) at about 288.3 eV. The O 1s peak in this spectrum also displays two main peaks assigned to oxygen in hydroxyl groups (O-H), and oxygen atoms in carbonyl or carboxyl groups (C=O or O-C=O). These oxygen-containing functional groups play a crucial role in the surface chemistry of the material, influencing its reactivity and interactions with the metal oxide centers.

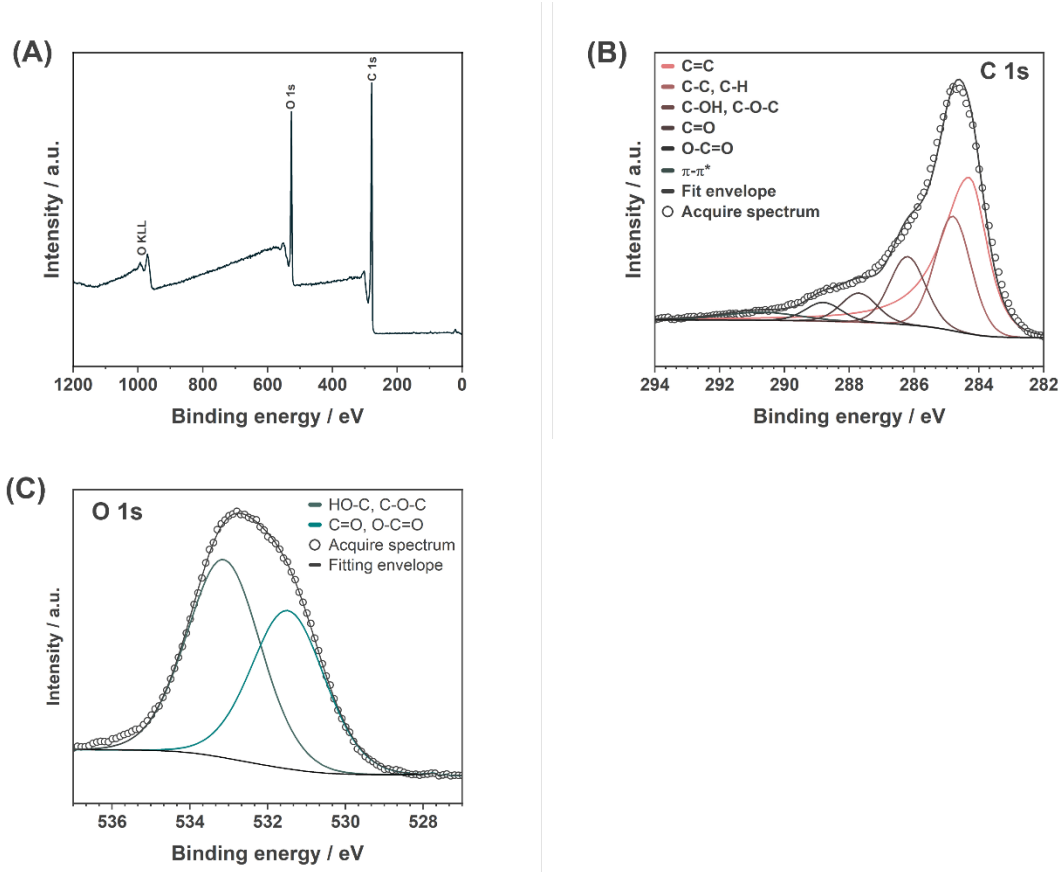

Figure S5. XPS data of *g*-C catalyst (**A**) survey scan and high-resolution spectra of (**B**) C 1s and (**C**) O 1s.

Table S5. Fitting parameters of *g*-C XPS data.

C 1s				
	BE / eV	**FWHM / eV**	**Line shape**	**% Area**
C=C	284.30	1.30	LA(1.2, 2.5, 5)	53.8
C–C, C–H	284.80	1.30	GL(30)	22.0
C–OH, C–O–C	286.20	1.30	GL(30)	15.9
C=O	287.70	1.30	GL(30)	5.4
O–C=O	288.80	1.30	GL(30)	2.9
π–π*	290.71	2.70	GL(30)	0
O 1s				
	BE / eV	FWHM / eV	Line shape	% Area
C=O, O–C=O	531.48	2.23	GL(30)	44.4
C–OH, C–O–C	533.13	2.23	GL(30)	55.6

XPS measurements of samples containing 1.6wt% and 32 wt% Fe/*g*-C samples were also performed and displayed in **Figure S6** and **S7**, respectively. The XPS spectra of C 1s and O 1s core levels were acquired to investigate the chemical composition of the samples in

more detail. The C 1s peak shows a decrease in carbon containing oxygen as the concentration of iron increases converting these groups into carbon-carbon network. The O 1s peak in both samples also displays a range of binding energy shifts indicative of different oxygen species on the sample's surface. These shifts can be associated with oxygen atoms bound to metal ions (metal oxides), oxygen in hydroxyl groups (O-H), and oxygen atoms in carbonyl or carboxyl groups (C=O or O-C=O).

The high-resolution XPS of Fe 2p was also measured for both 1.6 wt% and 32 wt% Fe/*g*-C (**Figure S6 D** and **S7 D**) samples. The deconvolution of the Fe 2p spectra revealed detailed information about the oxidation states of iron on the sample surfaces and provided insights into its chemical environment and coordination. From the deconvolution it was possible to determined that 33% of iron present in the 1.6wt% Fe/*g*-C sample is in the form of Fe_2O_3 and 67% in the form of Fe_3O_4. However, in the 32wt% Fe/*g*-C sample the concentration of iron photoactive specie (Fe_2O_3) increases with a total of 67% while 33% is in the form of Fe_3O_4. These results are also in agreement with XRD data presented in **Figure 2**.

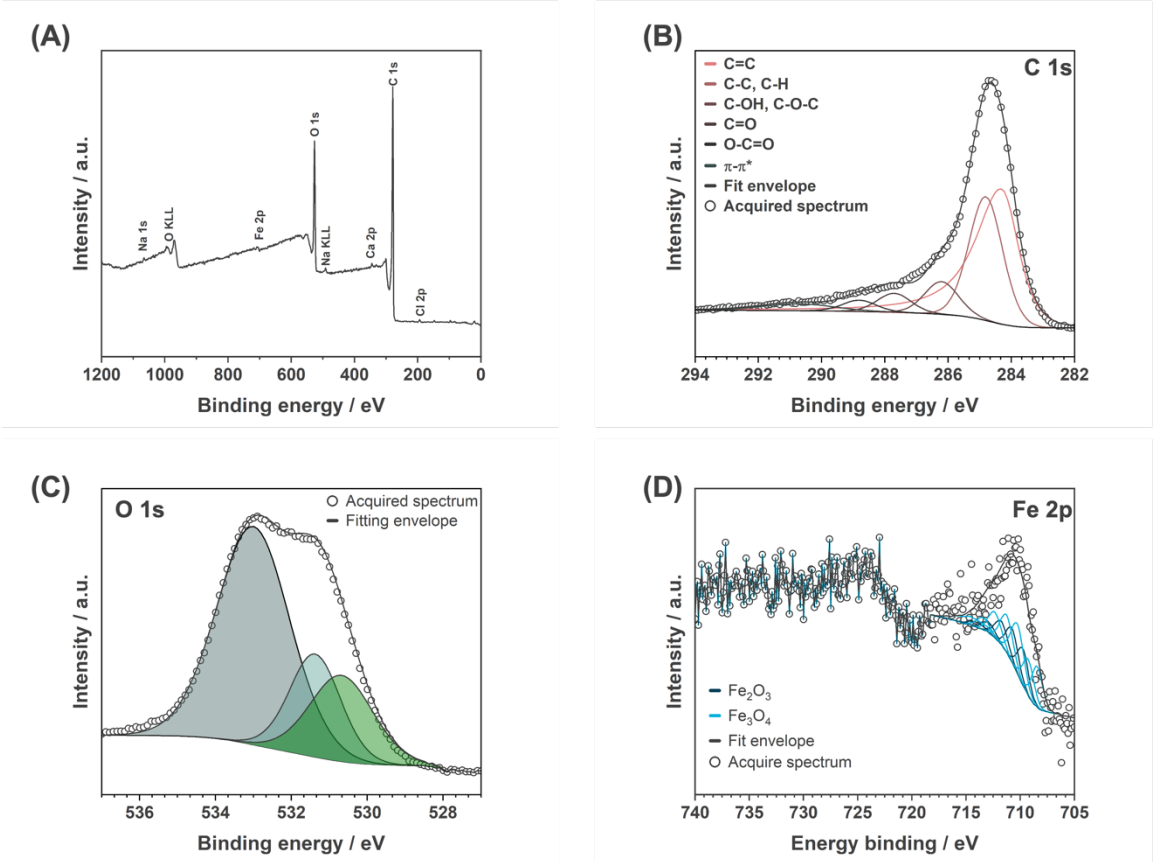

Figure S6. XPS data of 1.6wt% Fe/*g*-C catalyst (**A**) survey scan and high-resolution spectra of (**B**) C 1s, (**C**) O 1s and (**D**) Fe 2p.

Table S6. Fitting parameters of 1.6wt% Fe/*g*-C XPS data.

C 1s				
	BE / eV	**FWHM / eV**	**Line shape**	**% Area**
C=C	284.30	1.30	LA(1.2, 2.5, 5)	51.4
C–C, C–H	284.80	1.30	GL(30)	26.0
C–OH, C–O–C	286.20	1.30	GL(30)	13.7
C=O	287.70	1.30	GL(30)	5.4
O–C=O	288.80	1.30	GL(30)	3.5
π–π*	290.71	2.70	GL(30)	0
O 1s				
	BE / eV	**FWHM / eV**	**Line shape**	**% Area**
	531.48	2.23	GL(30)	44.4
	533.13	2.23	GL(30)	55.6
Fe 2p				
	BE / eV	**FWHM / eV**	**Line shape**	**% Area**
Fe_3O_4	708.45	1.20	GL(30)	11.2
Fe_3O_4	709.25	1.20	GL(30)	9.9
Fe_2O_3	709.75	1.20	GL(30)	10.1
Fe_3O_4	710.25	1.40	GL(30)	15.9
Fe_2O_3	710.75	1.30	GL(30)	10.1
Fe_3O_4	711.25	1.40	GL(30)	11.9
Fe_2O_3	711.75	1.40	GL(30)	7.5
Fe_3O_4	712.35	1.40	GL(30)	8.2
Fe_2O_3	712.95	1.40	GL(30)	3.4
Fe_3O_4	713.45	1.40	GL(30)	3.8
Fe_2O_3	714.05	1.70	GL(30)	1.9
Fe_3O_4	714.55	3.30	GL(30)	6.1

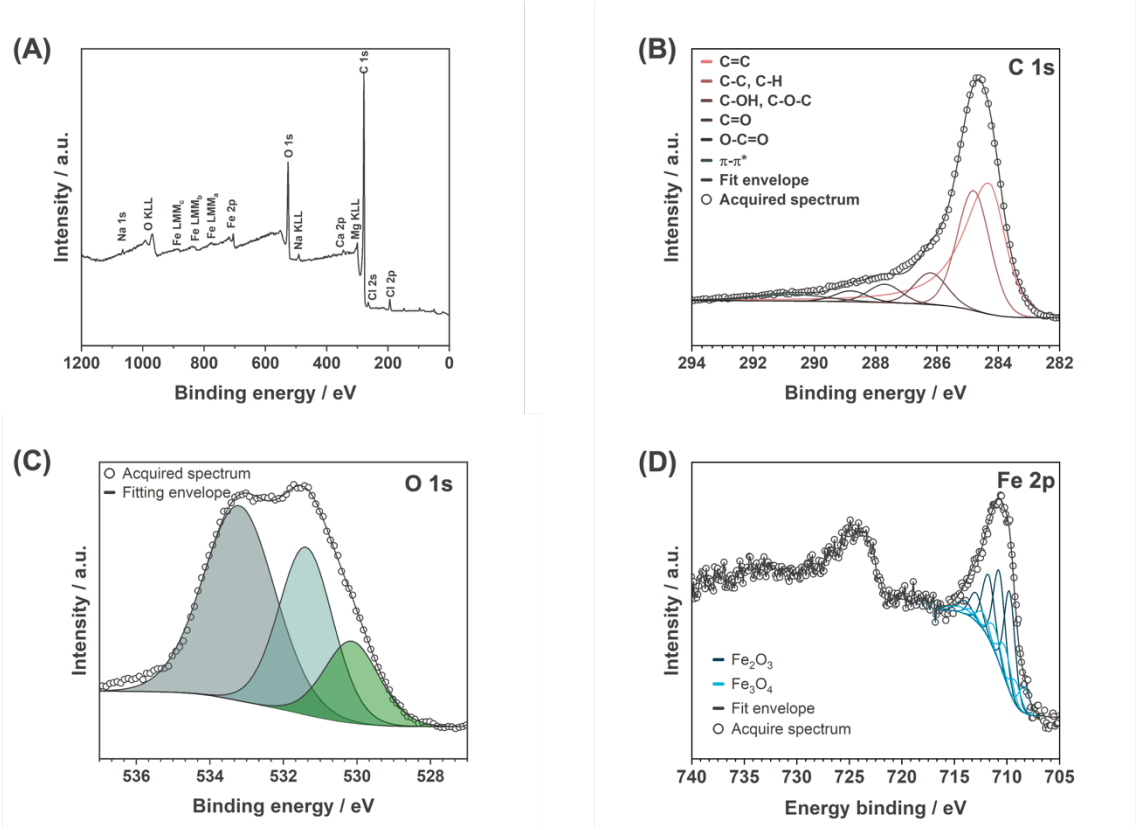

Figure S7. XPS data of 32wt% Fe/*g*-C catalyst (**A**) survey scan and high-resolution spectra of (**B**) C 1s, (**C**) O 1s and (**D**) Fe 2p.

Table S7. Fitting parameters of 32wt% Fe/*g*-C XPS data.

C 1s				
	BE / eV	**FWHM / eV**	**Line shape**	**% Area**
C=C	284.30	1.27	LA(1.2, 2.5, 5)	52.9
C–C, C–H	284.80	1.25	GL(30)	31.1
C–OH, C–O–C	286.20	1.25	GL(30)	8.3
C=O	287.70	1.25	GL(30)	4.8
O–C=O	288.80	1.25	GL(30)	2.9
π–π*	290.72	2.70	GL(30)	0
O 1s				
	BE / eV	**FWHM / eV**	**Line shape**	**% Area**
	531.48	2.23	GL(30)	44.4
	533.13	2.23	GL(30)	55.6
Fe 2p				
	BE / eV	**FWHM / eV**	**Line shape**	**% Area**
Fe_3O_4	708.35	1.20	GL(30)	5.5
Fe_3O_4	709.18	1.20	GL(30)	4.9

Fe_2O_3	709.75	1.20	GL(30)	20.6
Fe_3O_4	710.18	1.40	GL(30)	7.8
Fe_2O_3	710.75	1.30	GL(30)	20.6
Fe_3O_4	711.18	1.40	GL(30)	5.8
Fe_2O_3	711.75	1.40	GL(30)	15.3
Fe_3O_4	712.28	1.40	GL(30)	4.0
Fe_2O_3	712.95	1.40	GL(30)	6.8
Fe_3O_4	713.38	1.40	GL(30)	1.9
Fe_2O_3	714.05	1.70	GL(30)	3.8
Fe_3O_4	714.48	3.30	GL(30)	3.0

Table S8. Fitting parameters of O 1s high-resolution XPS spectra to monitor different oxygen species present on the photocatalyst surface during the cycles.

Before reaction				
	BE / eV	**FWHM / eV**	**Line shape**	**% Area**
lattice oxygen	530.2	1.30	GL(30)	4.9
OH groups	531.4	1.30	GL(30)	37.4
carbonyl groups	533.2	2.30	GL(30)	57.7
After cycle 1				
lattice oxygen	530.0	1.30	GL(30)	5.7
OH groups	531.3	1.30	GL(30)	13.2
carbonyl groups	532.2	2.30	GL(30)	81.1
After cycle 5				
lattice oxygen	529.9	1.30	GL(30)	5.2
OH groups	531.4	1.30	GL(30)	59.0
carbonyl groups	533.3	2.230	GL(30)	35.8

2. Photocatalytic Tests

2.1. Experimental setup

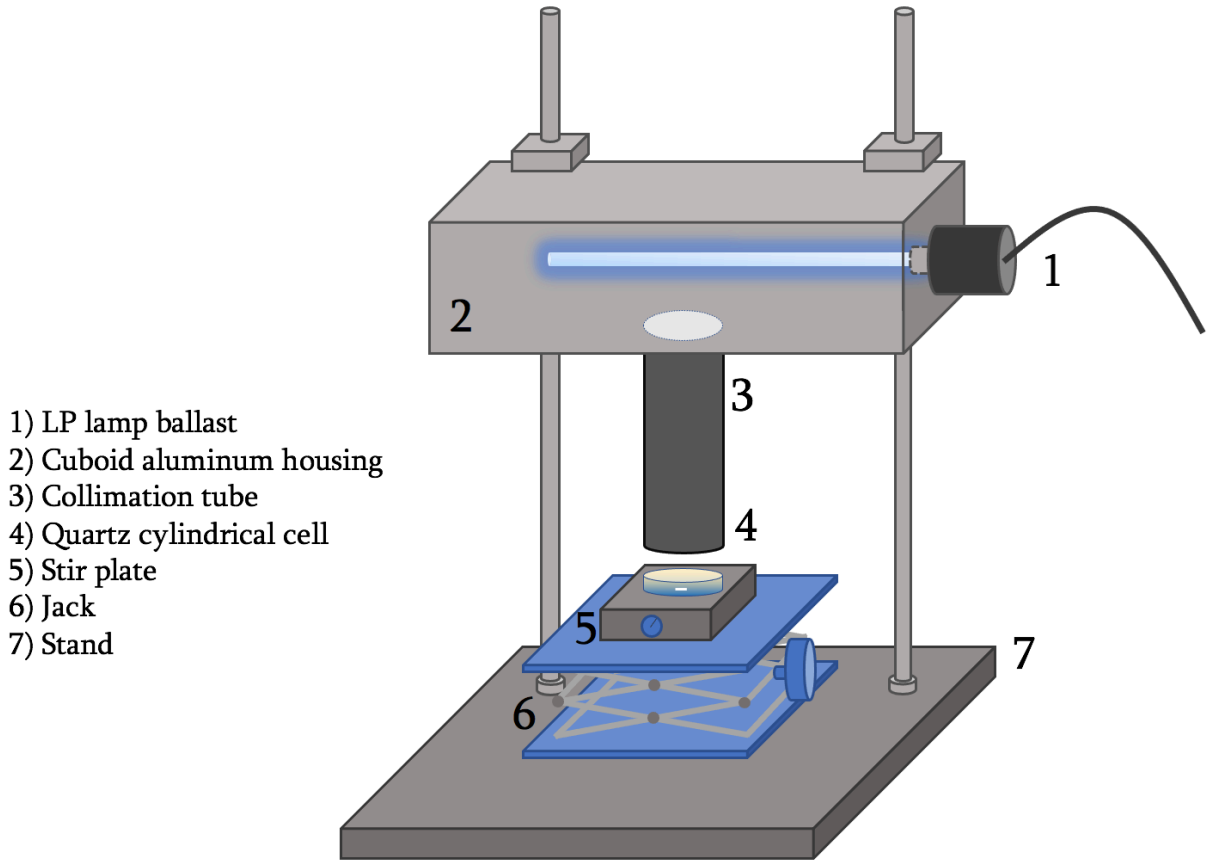

Figure S8. UV collimated beam photoreactor

3. Photocatalytic degradation of PFOA

Figure S9A shows PFOA removal efficiency under dark and UV processes within 6 h in different catalyst dosages (0.1-1 g/L). As shown, high dosage of catalyst favored removal of PFOA in both dark and UV processes since more adsorption sites are available for PFOA molecules, enhancing their adsorption and consequent decomposition. **Figure S9B** shows the kinetic of PFOA removal during UV/32wt%Fe/*g*-C process at different dosages of the catalyst.

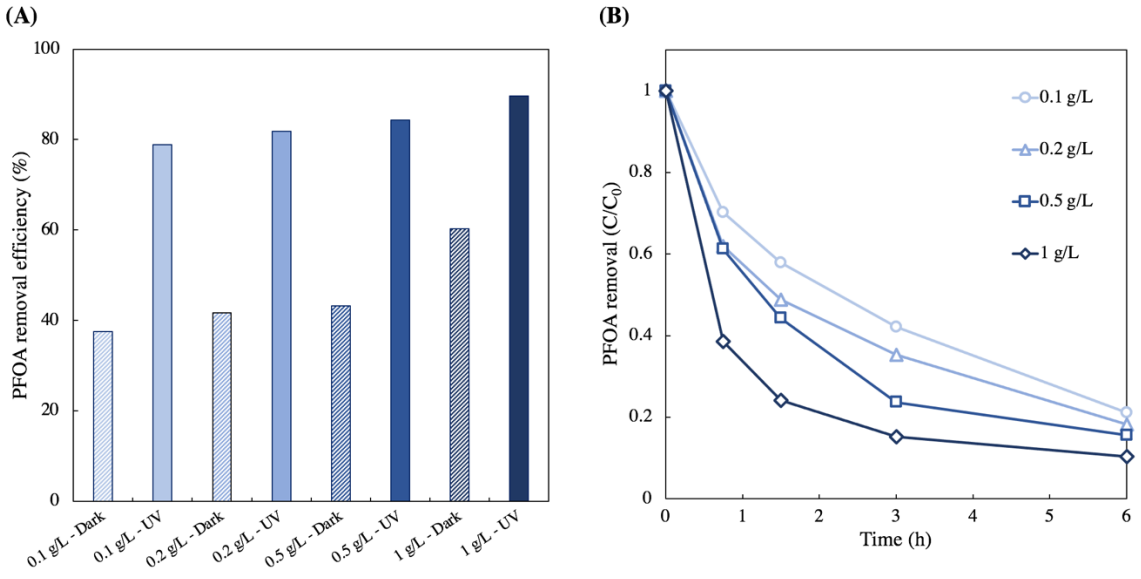

Figure S9. (A) Effects of catalyst dosage on PFOA removal in dark and UV systems. Experimental conditions: $[PFOA]_0$ = 1 mg/L, temperature = 22±2 ℃, and UV fluence rate in photochemical processes = 1.42±0.05 mW/cm^2. (B) PFOA removal in UV/32wt%Fe/*g*-C process. Experimental conditions: $[PFOA]_0$ = 1 mg/L, temperature = 22±2 ℃, and UV fluence rate = 1.42±0.05 mW/cm^2.

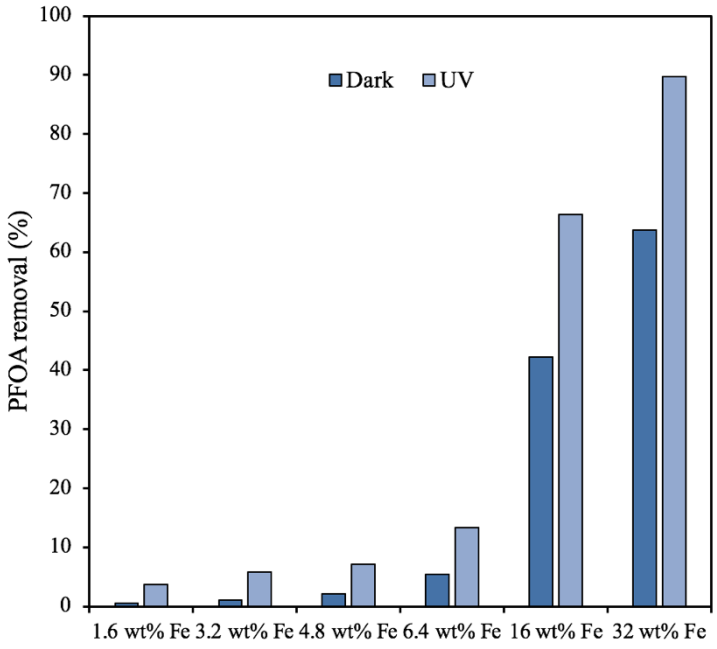

Figure S10. PFOA removal in dark and UV conditions using g-C photocatalysts with varying concentrations of iron doping.

Figure S11 compared the removal efficiency of PFOA under dark and UV process using high dosage of catalyst (1 g/L), highlighting the promising sorption and photo-catalytic activities of the catalyst.

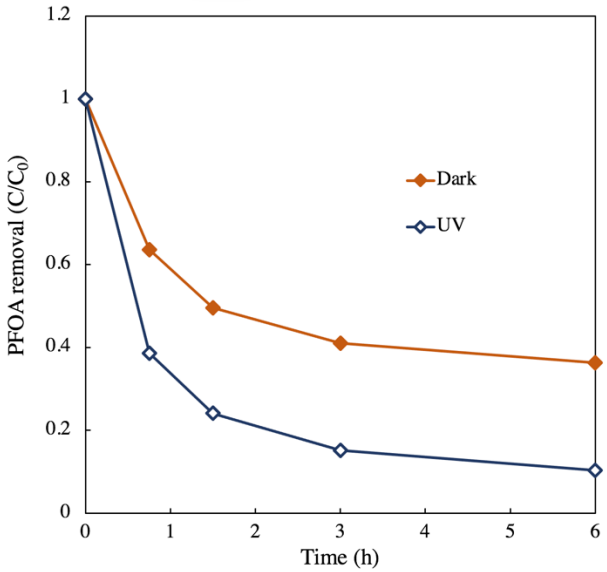

Figure S11. PFOA removal in dark and UV systems. Experimental conditions: $[PFOA]_0$ = 1 mg/L, temperature = 22±2 ℃, catalyst dosage = 1 g/L, and UV fluence rate in photochemical processes = 1.42±0.05 mW/cm^2.

Figure S12 illustrates the removal efficiency of PFOA within 6 h under dark and UV processes across varying initial concentrations (0.1-5 ppm). Notably, an increase in the initial concentration of PFOA led to a decrease in removal efficiency for both processes. For instance, at an initial concentration of 0.1 ppm, 94.4% and 99.4% of PFOA was removed within 6 hours in dark and UV processes, respectively. Conversely, at an initial concentration of 5 ppm, these percentages dropped to 60.7% and 85.6%, respectively. This trend is primarily attributed to the heightened competition of PFOA molecules for available sorption sites on the photocatalyst when PFOA concentration is elevated. Additionally, increasing the iron concentration from 32wt% to 64wt% did not enhance the photodegradation of PFOA, suggesting that the 32wt% Fe content is optimal for the process. This observation underscores the importance of finding the right balance in catalyst composition to achieve optimal performance.

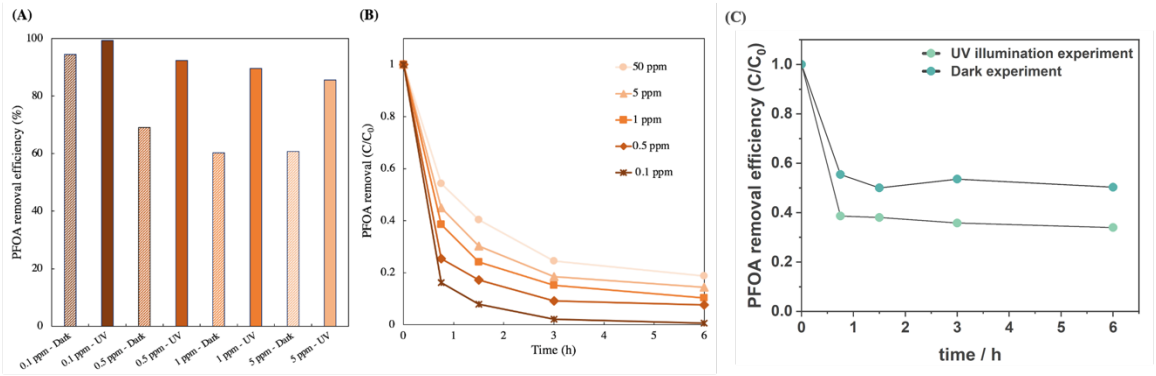

Figure S12. A) PFOA removal within 6 h in dark and UV processes in different initial concentrations of PFOA (0.1-5 ppm). B) Kinetic of PFOA removal at different initial concentrations during UV/32wt%Fe/*g*-C process. C) PFOA removal within 6 h in dark and UV process with 64wt% Fe/*g*-C photocatalyst. Experimental conditions: temperature = 22±2 ℃, catalyst dosage = 1 g/L, and UV fluence rate in photochemical process = 1.42±0.05 mW/cm^2.

Figure S13 A and **B** show the concentration profile of PFOA and its generated intermediates during UV/32wt%Fe/*g*-C process. As shown, shorter chain perfluorocarboxylic acids (PFCAs, $C_nF_{2n+1}COO^-$) with n from 2 to 6 (m/z ratios of 163 to 363) were the main intermediates generated during decomposition of PFOA. As shown, concentration of intermediates with longer chain length were higher than those with shorter chain length, implying stepwise formation of the generated intermediates. Evolution of intermediates proposed that the decomposition of PFOA involved cleavage of carboxylic functional group (COO^-) through UV irradiation of generated complex between COO^- and ferric on catalyst surface. Then, the generated $^{\bullet}C_nF_{2n+1}$ reacts with water or $^{\bullet}OH$ to generate unstable perfluorinated alcohol and then undergoes HF elimination and hydrolysis to generate the PFCA with one less CF_2 unit. The intermediate $C_{n-1}F_{2n-1}COO^-$ is further decomposed to shorter chain PFCAs in a similar pathway.

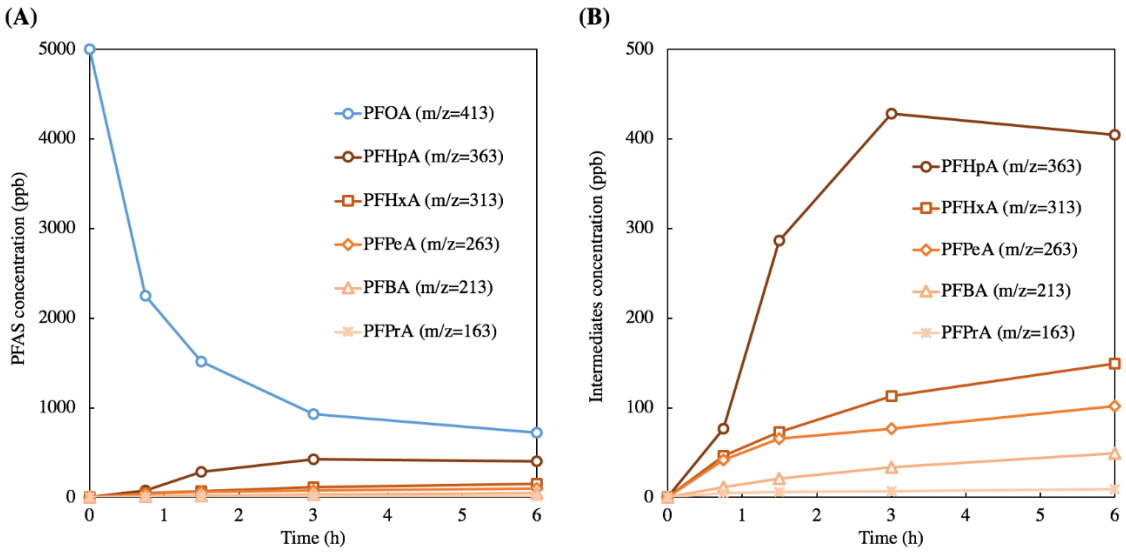

Figure S13. Concentration profile of PFOA and its generated intermediates in UV/32wt% Fe/*g*-C photocatalyst. Experimental conditions: $[PFOA]_0$ = 5 mg/L, catalyst dosage = 1 g/L, temperature = 22±2 °C, and UV fluence rate = 1.42±0.05 mW/cm^2.

Figure S14A shows the total fluorine recovery, i.e., the molar ratio of total fluorine in the form of PFOA, its generated intermediates (shorter chain PFCAs), and fluoride (F^-), versus time. The fluorine recovery using initially decreased to 42.2% within 1.5 hours, stabilizing thereafter. This is notably lower compared to our previous findings with a molecular photo-mediator (UV/VUV/sulfite system)[16], where fluorine recovery exceeded 90% at all irradiation times. The decrease is likely attributed to the adsorption of generated fluoride onto the catalyst surface. In a control experiment using sodium fluoride (NaF) with the same fluoride concentration as in 5 ppm PFOA (3.45 ppm F^-), we observed that 42.6 and 47.0% of the initial fluoride was adsorbed onto the catalyst surface (32 wt% Fe/g-C) in dark and UV processes, respectively (**Figure S14B**). This is primarily due to the presence of iron oxide on the catalyst surface, as no fluoride adsorption was noted using pure g-C catalyst.

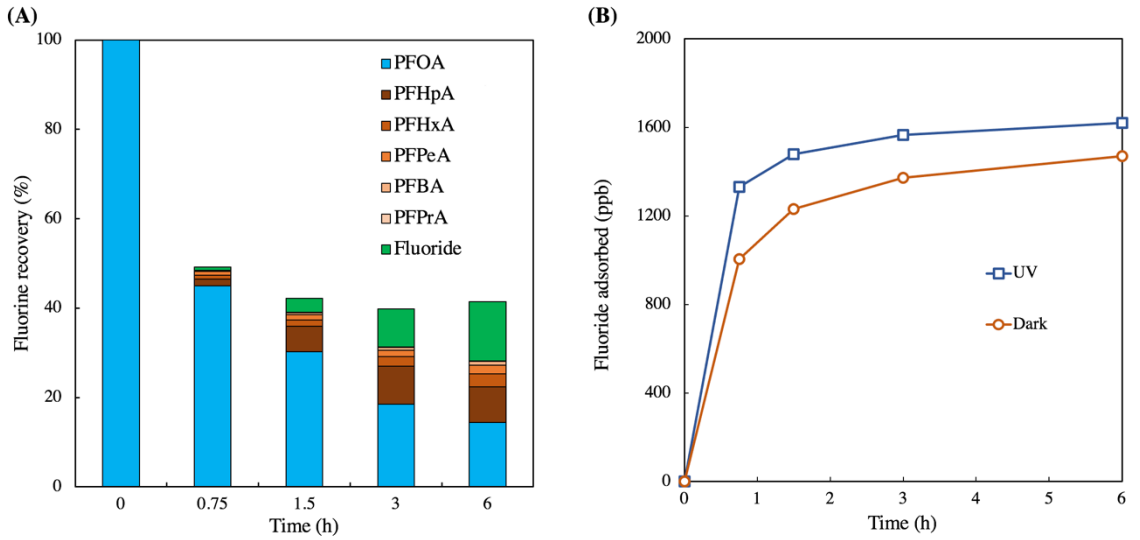

Figure S14. A) Fluorine mass balance during PFOA removal using UV/32wt% Fe/*g*-C photocatalyst. Experimental conditions: $[PFOA]_0$ = 5 mg/L, catalyst dosage = 1 g/L, temperature = 22±2 °C, and UV fluence rate = 1.42±0.05 mW/cm^2. B) Adsorption of fluoride on catalyst surface in both dark and UV conditions. Experimental conditions: $[fluoride]_0$ = 3.5 mg/L, catalyst 32wt% Fe/g-C dosage = 1 g/L, temperature = 22±2 °C, and UV fluence rate in photochemical process = 1.42±0.05 mW/cm^2.

Figure S15 compares the removal of PFOA using UV/ferric (100 µM) as a molecular photo-mediator in its common concentration applied in earlier studies[17,18] and UV/32wt% Fe/*g*-C (1 g/L) photocatalyst. As shown, 63.8% and 89.7% of PFOA was removed in the presence of UV/ferric and UV/32wt% Fe/*g*-C within 6 h, respectively. Thus, compared to molecular photo-mediator, the photocatalyst employed in this study not only can be easily separated from the solution (eliminating sophisticated secondary chemical treatment of removing excess ferric sulfate), but also achieve significantly higher removal of PFOA.

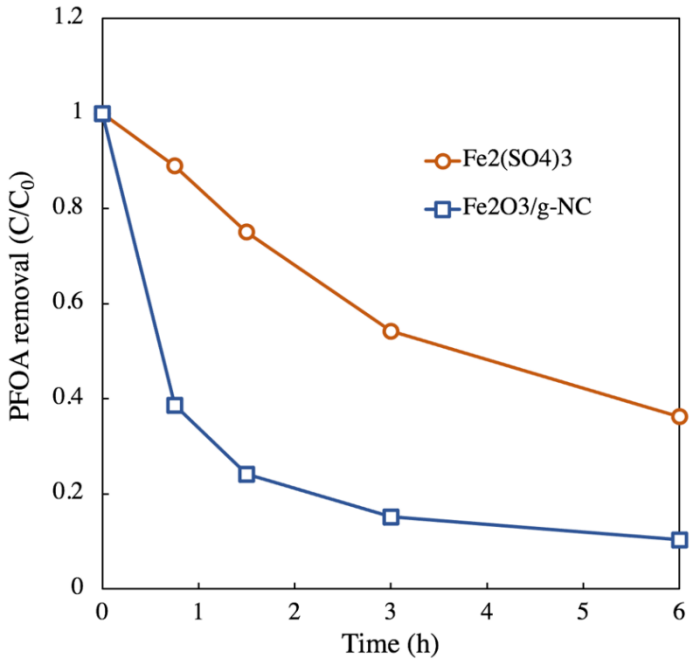

Figure S15. PFOA removal in UV/$Fe_2(SO_4)_3$ and UV/32wt%Fe/*g*-C systems. Experimental conditions: $[PFOA]_0$ = 1 mg/L, photocatalyst UV/32wt% Fe/g-C dosage = 1 g/L, $Fe_2(SO_4)_3$ dosage = 100 μM, temperature = 22±2 ℃, and UV fluence rate = 1.42±0.05 mW/cm^2.

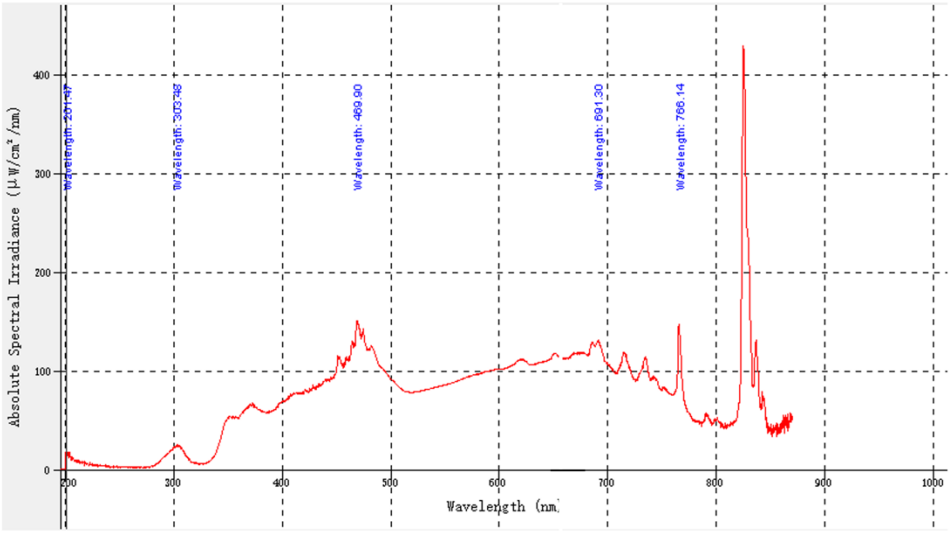

Figure S16. Absolute spectral irradiance (μW/cm^2/nm) of the employed sun simulator source versus wavelength.

References:

1. Shang, E. *et al.* Photocatalytic degradation of perfluorooctanoic acid over Pb-BiFeO3/rGO catalyst: Kinetics and mechanism. *Chemosphere* **211**, 34–43 (2018).
2. Sahu, S. P. *et al.* Rapid Degradation and Mineralization of Perfluorooctanoic Acid by a New Petitjeanite Bi3O(OH)(PO4)2 Microparticle Ultraviolet Photocatalyst. *Environmental Science and Technology Letters* **5**, 533–538 (2018).
3. Xu, T. *et al.* Enhanced photocatalytic degradation of perfluorooctanoic acid using carbon-modified bismuth phosphate composite: Effectiveness, material synergy and roles of carbon. *Chemical Engineering Journal* **395**, (2020).
4. Li, F. *et al.* A concentrate-and-destroy technique for degradation of perfluorooctanoic acid in water using a new adsorptive photocatalyst. *Water Research* **185**, 1–14 (2020).
5. Chen, M. J., Lo, S. L., Lee, Y. C. & Huang, C. C. Photocatalytic decomposition of perfluorooctanoic acid by transition-metal modified titanium dioxide. *Journal of Hazardous Materials* **288**, 168–175 (2015).
6. Li, X. *et al.* Efficient photocatalytic decomposition of perfluorooctanoic acid by indium oxide and its mechanism. *Environmental Science and Technology* **46**, 5528–5534 (2012).
7. Huang, D., Yin, L. & Niu, J. Photoinduced Hydrodefluorination Mechanisms of Perfluorooctanoic Acid by the SiC/Graphene Catalyst. *Environmental Science and Technology* **50**, 5857–5863 (2016).
8. Tian, H., Gao, J., Li, H., Boyd, S. A. & Gu, C. Complete Defluorination of Perfluorinated Compounds by Hydrated Electrons Generated from 3-Indole-acetic-acid in Organomodified Montmorillonite. *Scientific Reports 2016 6:1* **6**, 1–9 (2016).
9. Bao, Y. *et al.* Degradation of PFOA Substitute: GenX (HFPO-DA Ammonium Salt): Oxidation with UV/Persulfate or Reduction with UV/Sulfite? *Environmental Science and Technology* **52**, 11728–11734 (2018).
10. Song, Z., Tang, H., Wang, N. & Zhu, L. Reductive defluorination of perfluorooctanoic acid by hydrated electrons in a sulfite-mediated UV photochemical system. *Journal of Hazardous Materials* **262**, 332–338 (2013).
11. Guo, C. *et al.* Synergistic impact of humic acid on the photo-reductive decomposition of perfluorooctanoic acid. *Chemical Engineering Journal* **360**, 1101–1110 (2019).
12. Thi, L. A. P., Do, H. T., Lee, Y. C. & Lo, S. L. Photochemical decomposition of perfluorooctanoic acids in aqueous carbonate solution with UV irradiation. *Chemical Engineering Journal* **221**, 258–263 (2013).
13. Wang, Y., Zhang, P., Pan, G. & Chen, H. Ferric ion mediated photochemical decomposition of perfluorooctanoic acid (PFOA) by 254 nm UV light. *Journal of Hazardous Materials* **160**, 181–186 (2008).
14. Qian, Y. *et al.* Perfluorooctanoic Acid Degradation Using UV-Persulfate Process: Modeling of the Degradation and Chlorate Formation. *Environmental Science and Technology* **50**, 772–781 (2016).
15. Cao, M. H. *et al.* Photochemical decomposition of perfluorooctanoic acid in aqueous periodate with VUV and UV light irradiation. *Journal of Hazardous Materials* **179**, 1143–1146 (2010).
16. Esfahani, E. B. & Mohseni, M. Fluence-based photo-reductive decomposition of PFAS using vacuum UV (VUV) irradiation: Effects of key parameters and decomposition mechanism. *Journal of Environmental Chemical Engineering* **10**, 107050 (2022).

17. Jin, L., Zhang, P., Shao, T. & Zhao, S. Ferric ion mediated photodecomposition of aqueous perfluorooctane sulfonate (PFOS) under UV irradiation and its mechanism. *Journal of Hazardous Materials* **271**, 9–15 (2014).
18. Wang, Y., Zhang, P., Pan, G. & Chen, H. Ferric ion mediated photochemical decomposition of perfluorooctanoic acid (PFOA) by 254 nm UV light. *Journal of Hazardous Materials* **160**, 181–186 (2008).